JOURNAL OF MATERIALS SCIENCE **38** (2003) 2517–2523

The effects of fluid flow on secondary arm coarsening during dendritic solidification

ANDREW M. MULLIS
Department of Materials, University of Leeds, Leeds LS2 9JT, UK
E-mail: metcam@sun.leeds.ac.uk

Although dendrites are the result of diffusion limited growth it has long been appreciated that flow within the parent melt can have a dramatic effect on these structures. A free boundary model of dendritic solidification is used to assess the effects on the secondary arm coarsening processes of fluid flow within the parent melt. It is found that for solutally controlled coarsening realistic interdendritic flow velocities of the order 10^{-3}–10^{-2} m s^{-1} give rise to ripening rates which are comparable to diffusive transport. However, only flows with a component aligned from the secondary tip towards the root enhance the ripening rate. Oppositely aligned flows actually reduce the ripening rate. Thus, due to the four-fold symmetry of dendrites in cubic metals, the actual effect on the secondary arm spacing could be quite small. The results are shown to be in general agreement with recent microgravity experiments on dendritic coarsening.

1. Introduction

One of the most fundamental and all pervasive microstructures produced during the solidification of metals is the dendrite. Remnants of these dendritic microstructures often survive subsequent processing operations, such as rolling and forging, and the length scales established by the dendrite can influence not only the final grain size but also micro- and hence macrosegregation patterns. This can have a wide-ranging influence on both the properties of finished metallic products, affecting for instance mechanical properties, corrosion resistance and surface finish, and on the formability of metallic feedstock, such as the ability to resist hot tearing during rolling.

Where dendritic growth has been observed directly, in transparent analogue casting systems such as succinonitrile [1] and xenon [2], the evidence is that the morphology of dendrites grown at different undercoolings is probably self-similar when scaled against the tip radius, R. Consequently, many of the more obvious length scales of the dendrite (trunk radius, primary spacing etc.) are simple multiples of R. Two length scales may thus be defined which characterize the dendritic solidification. One is the tip radius, R, the other is the secondary arm spacing, λ_2. While R is a function of the growth conditions, it is well established that secondary dendrite arm spacing is determined primarily by coarsening processes [3, 4].

Experimentally, the kinetics of the coarsening process can be represented [5] via the relationship

$$\lambda_2 = ct_s^n \tag{1}$$

where t_s the local solidification time, that is the time for which the solid and liquid co-existed, and c is a constant. The exponent n has generally been found [6] to be around 1/3. Theoretically, both radial melting of the smaller arms [7] and lateral melting of the smaller arms from their tips downwards [6] has been found to give the correct form of the scaling law. However, *in situ*, observations of the coarsening process in the analogue casting system NH_4Cl-H_2O by Kahlweit [8] found that smaller sidearms are always removed from their tips downwards, indicating that lateral dissolution is the dominant process.

Dendrites are diffusive structures, that is the formation of dendrites is indicative of diffusion limited transport of heat and/or solute. However, it has been recognized for many years that fluid flow within a melt can have profound effects on the morphology of dendritic growth. One of the first unambiguous demonstrations of this was provided in a series of images by Glicksman *et al*. [9] of dendritic growth in the transparent succinonitrile-argon system. They found that secondary arm development is asymmetric for growth in the terrestrial laboratory and that as the principal growth direction is rotated with respect to the $\boldsymbol{g}$-vector, the growth of side arms aligned (root to tip) with the $\boldsymbol{g}$-vector is favoured. They also found that orientation with respect to the $\boldsymbol{g}$-vector could effect the secondary arm spacing, λ_2. Convection induced flow was found to be important at low undercoolings, with the effects diminishing to zero as the undercooling was increased.

At low growth rates it is almost impossible to inhibit natural convection during solidification in the terrestrial laboratory. Consequently, one of the most fruitful approaches to studying convection-induced effects has been the utilisation of microgravity solidification. A number of early microgravity solidification experiments [10–14] conducted during parabolic aircraft flights and on sounding rockets indicated that both primary, λ_1, and secondary dendrite arm spacing

increased in microgravity, when compared with similar samples solidified at 1-g. Typically, microgravity experiments have reported secondary arm spacings 20–50% greater than that found at 1-g although one study [15], on the Ni-based superalloy PWA-1480, found that λ_2 increased by a factor of 20. However, interpretation of these early results was somewhat muddled for a number of reasons. Firstly, as described above, primary and secondary dendrite spacing are determined by completely different processes. Consequently, it is not clear why λ_1 and λ_2 should respond in the same way to the suppression of convection. Secondly, coarsening might be expected to be promoted by the enhanced heat and mass transport engendered by convection, leading to λ_2 being larger in 1-g rather than in microgravity.

Many of these issues were resolved by the Isothermal Dendrite Growth Experiment [16] (IDGE), in which dendritic growth of high purity succinonitrile was studied under microgravity conditions in the cargo bay of the Space Shuttle Columbia as part of the second United States Microgravity Payload (USMP-2). Sidebranch spacings were measured and the measurements were classified as belong to either the uniform regime, the region close to the tip in which initial sidebranch perturbations form but coarsening is negligible, or the coarsening regime. The boundary between these two regimes was placed at around 30–33R. An analysis of the IDGE data by Corrigan *et al*. [1] showed that, when scaled against the dendrite tip radius, no statistically significant difference existed between λ_2 as measured in microgravity and a terrestrial data set acquired under identical conditions apart from the gravity environment. The apparent discrepancy between this result and other measurements of secondary arm spacing in microgravity can be explained with reference to the findings of Koss *et al*. [17] who found that the measured dendrite tip radius was systematically higher in the microgravity experiments than in comparable terrestrial experiments. Moreover, the microgravity data set accord well with theory for diffusion limited growth and it must be concluded the difference between the data sets is result of enhanced transport at the dendrite tip due to convection in the 1-g data set. Consequently, most previous observations that secondary dendrite arm spacing increases under microgravity conditions can be explained by postulating the growth of self-similar dendrites at a larger tip radius. Nonetheless, as secondary dendrite arm spacing is governed by a (transport limited) ripening process, it is unlikely that buoyancy driven flow has no effect other than to reduce the overall scale of the dendritic structure via a reduction of the tip radius. It may be the case that the effect on secondary arm spacing has generally been masked by the much larger effect on the tip radius. However, some flow related effects were found in the data of Corrigan *et al*. [1]. When the dendrite envelope was parameterized via the relationship

$$\frac{X}{R} = \alpha\left(\frac{Z}{R}\right)^{\beta} \tag{2}$$

where (X, Z) are the co-ordinates of the sidebranch tips in a frame of reference with its origin at the tip of the primary dendrite (primary growth along x), it was found that statistically significant differences existed between the microgravity and 1-g data sets for both α and β, although it is not clear that this is specifically related to coarsening. A detailed analysis of envelope shapes and their relationship to dendrite growth models is given by Li and Beckermann [18].

The IDGE results have also some yielded a number of results that suggest dendritic coarsening may not yet be fully understood, even in the purely diffusive microgravity environment. In particular, Li and Beckermann [19] find that in the coarsening regime the secondary arm spacing, λ_2, does not appear to follow the usual $t_s^{1/3}$ relationship, although the radius of curvature at the secondary arm root is well described by current ripening theories. They suggest that this discrepancy could be due to the fact that for free dendritic growth there is a competition between capillary driven ripening and net solidification due to the presence of the undercooled melt.

The complexity of the solidification process is such that, until recently, models of solidification in a non-stationary fluid have generally decoupling the flow from the evolution of the interface [20]. However, recently a number of authors have presented 2-dimensional phase-field models including the effects of flow [21–24]. In general these have concentrated on the effect of flow on the tip shape, growth velocity [23] and the formation of initial side-branch perturbations [21, 24]. However, in a study on the effects of a shear flow on the primary dendrite morphology Tönhardt and Amberg [21] note that where the flow is aligned from tip to root with secondary dendrite arms ripening appears to be increased, although they do not quantify the effect. Beckermann *et al*. [25] and Diepers *et al*. [26] have presented a model for the Ostwald ripening of a population of infinitely long cylinders in a flow-field, in which they find that flow changes the time dependence of the coarsening rate. Diepers *et al*. calculated the coarsening rate on two different bases, the time evolution of the mean radius of curvature and the time evolution of the specific surface area. The coarsening rate for pure diffusive transport was found to be $t_s^{1/3}$, irrespective of the calculation basis used. In the presence of flow the coarsening rate was found to be $t_s^{1/2}$ if calculated on an area basis and to fall between $t_s^{1/3}$ and $t_s^{1/2}$ if calculated on a curvature basis. However, as experimentally dendrites are always observed to coarsen by lateral, rather than radial, dissolution the implications of this result for dendritic coarsening are not clear.

In this paper we use a free boundary model of dendritic solidification to assess the effects of flow on the dynamics of secondary arm coarsening. Flow both parallel to and perpendicular to the axis of the secondary arm is considered. The results of the simulations are discussed with reference IDGE microgravity experiment.

2. Computational procedure

We consider here thermal ripening although the case of solutal ripening of a pure material grown from solution

is directly analogous. Heat and mass transfer within the dendritic array is governed by the diffusion equation

$$\frac{\partial T}{\partial t} = D\nabla^2 T \tag{3}$$

where T is temperature and t is time. D is a composite thermal diffusivity given by

$$D = pD_s + (1-p)D_l \tag{4}$$

where D_s is the thermal diffusivity in the solid, D_l is the thermal diffusivity in the liquid and p is an order parameter which takes values $0 \le p \le 1$, where $p = 1$ denotes the material being fully solid and $p = 0$ fully liquid. Balance of fluxes at the solid-liquid interface is given by

$$H\rho v = \kappa_s G_s - \kappa_l G_l \tag{5}$$

where ρ is the density, taken here as being the same in the solid and liquid states, H is the latent heat of fusion, κ_s and κ_l are the thermal conductivities in the solid and liquid respectively, v is the local velocity of the interface along the outward pointing normal $\hat{n}$, and G_s and G_l are the thermal gradients at the interface along $\hat{n}$ in the solid and the liquid.

Solutions to the diffusion problem are sought on a regular, 2-dimensional $M \times N$ grid using a alternating direct implicit (ADI) finite difference scheme [27] to yield the temperature at the advanced time step.

The interface temperature is fixed by its geometry. For a solid growing with an anisotropic, four-fold symmetric interfacial energy γ, the local interface liquidus temperature, T_i, is given by

$$T_i = T_m - \frac{(K_1 + K_2)\gamma_o T_m}{H\rho}\{1 - a\cos(4\phi)\} \tag{6}$$

where γ_o is the nominal interfacial energy between the solid and liquid phases, a the surface energy anisotropy, ϕ the angle between $\hat{n}$ and the principal crystallographic axes and T_m is the equilibrium liquids temperature. K_1 and K_2 are the two principal components of the surface curvature. If y is the locus of the solidification front then K_1 is given by

$$K_1 = \frac{y''}{\{1 + (y')^2\}^{3/2}} \tag{7}$$

However, for a 2-dimensional model the K_2 component of curvature would normally be absent, although this can have a significant impact on ripening kinetics. For a figure of revolution K_2 is given (in cylindrical coordinates) by

$$K_2 = \frac{y'}{r(1 - (r')^2)^{1/2}} \tag{8}$$

where r is the radial distance from the rotation axis to the corresponding point on the locus y. Here we have employed a pseudo 3-dimensional model. During the ripening process the dendrites maintain a good degree of symmetry about the axis passing through the tip and consequently we treat each needle as if it were a figure of revolution about a local rotational axis located at x_c,

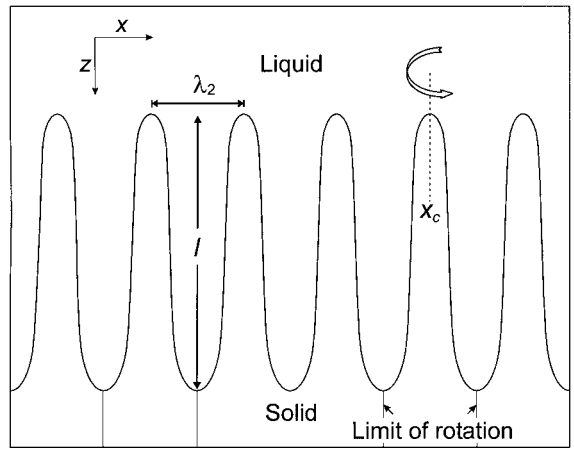

Figure 1 Schematic diagram of the model array of secondary dendrite arms used in the simulations.

as shown in Fig. 1. The component of curvature K_2 is then evaluated as

$$K_2 = \frac{y'}{(x - x_c)(1 - (x')^2)^{1/2}} \tag{9}$$

The solution to the diffusion equation remains however 2-dimensional.

In order to simulate solidification and melting the model independently tracks the order parameter $p_{m,n}$ at each grid point. If at any node (m,n) $0 < p_{m,n} < 1$, the volume cell which has that node as its centroid will contain some part of the freezing front and the temperature at that node is fixed at the local liquidus temperature. At the end of each time step $p_{m,n}$ is updated at each node for which $0 < p_{m,n} < 1$ by considering the heat flux into or out of the volume element during the time step.

However, unlike the phase field approach pioneered by Kobayashi [28], in which the solidification front is assumed diffuse, here we assume the solidification front is sharp and must have a definite position. Consequently we interpret a value of $0 < p_{m,n} < 1$ as meaning the volume cell which has the node (m,n) as its centroid contains some part of the front such that the area fraction of solid contained within the cell is just equal to $p_{m,n}$. In this case the differentials of the locus of the freezing front, y, are given by

$$y' = p'_{m,n} = \frac{(p_{m+1,n} - p_{m-1,n})\delta z}{2\delta x} \tag{10}$$

and

$$y'' = p''_{m,n} = \frac{(p_{m+1,n} - 2p_{m,n} + p_{m-1,n})\delta z}{(\delta x)^2} \tag{11}$$

Full details of the computational procedure are given by Mullis [29].

Analyzing flow effects in a 2-dimensional model and then attempting to use that model to explain inherently 3-dimensional phenomena presents serious problems as the nature of the 2- and 3-dimensional flow fields may be very different. In particular, for the geometry shown in Fig. 1, in the 2-dimensional model flow in the x-direction would be completely blocked in the interdendritic region by the dendrites while in the actual

3-dimensional physical system flow around the dendrite would occur. To attempt to build into the model an approximate flow field which overcomes this problem, without moving to a full 3-dimensional treatment which is currently computational infeasible, we have adopted the following procedure. The domain is subject to what we term a uniformly directed flow field, which is a flow field generated on the basis of a number of empirical rules.

The first stage in generating the uniformly directed flow field is to use a commercial computational fluid dynamics package to simulate the flow around a representative 3-dimensional body. In this case we used the program CFX 4.1[1] to generate the flow-field around a paraboloid of revolution in 3-dimension at Reynolds numbers that are appropriate to interdendritic flow and in the same orientation as the flow to be simulated in the 2-dimensional free boundary model. The magnitude of the flow velocity is then parameterized in terms of the parameters X/R and Z/R where X and Z are co-ordinates in a frame of reference with its origin at the dendrite tip. This parameterization is then used in the 2-dimensional free boundary model to generate the flow-field $\boldsymbol{V}_{\mathbf{f}}$. Fluid enters the domain with an initial velocity ($U_{fx}\hat{i}$, $U_{fz}\hat{k}$) and maintains this velocity far from the solid. However in proximity to the dendrites the magnitude of $\boldsymbol{V}_{\mathbf{f}}$ is reduced according to the parameterization derived from the 3-D flow model, although we do not attempt to parameterize the direction of the flow. This results in a flow within the 2-D model which has a number of desirable features namely;

- the flow velocity is unaltered far from the solid,
- the flow velocity varies smoothly towards zero as a solid interface is approached, simulating the no-slip condition, and is zero in the solid,
- a non-zero flow occurs in the interdendritic region as the 2-D dendrites do not completely block the flow.

The computational domain within the free boundary is extended sufficiently far beyond the initial dendrite tips in the z-direction that the flow-field on the upper z boundary may be considered to be unperturbed by the presence of the solid. The flow velocity on the upper z boundary is then just equal to the inlet velocity. In most simulations the total z extent was taken as 2.5 times the initial dendrite amplitude (note that only the part of the domain showing solid is shown in Fig. 1).

Within the model the effects with a uniformly directed flow field are incorporated by rewriting the transport equation (Equation 3) as

$$\frac{\partial T}{\partial t} = D\nabla^2 T - \boldsymbol{V}_{\mathbf{f}} \cdot \left(\frac{\partial}{\partial x}\hat{i} + \frac{\partial}{\partial z}\hat{j} \right) T \qquad (12)$$

where $\boldsymbol{V}_{\mathbf{f}}$ is the local fluid velocity.

As a consequence of our free boundary solution to the diffusion equation being 2-dimensional it is likely that the calculated ripening rates will be slower than those pertaining in 3-dimensions. However, as all our transport processes are calculated in 2-dimensions we should still be in a position to comment upon the relative rates of flow and diffusional transport and we will return to this issue when discussing the results of the simulations.

In order to study the dendritic ripening problem, including the effects of flow, we use a model dendritic array as illustrated in Fig. 1, consisting of a region of the primary trunk containing seven secondary arms of identical curvature R_2. Each of the arms has length l. By tracking the position of the secondary tips as a function of time, the average ripening rate for the array, $\mathrm{d}l/\mathrm{d}t$, can be estimated. The results are presented initially in a non-dimensional form so that the conclusions can be generalized to either thermal or solutal growth. For the same reason we consider ripening in both the symmetric ($D_\mathrm{s} = D_\mathrm{l}$) and asymmetric ($D_\mathrm{s} = 0$) models, where $D_\mathrm{s} = D_\mathrm{l}$ are the diffusivities in the solid and liquid phase respectively.

3. Results

As discussed above, studies of ripening in transparent analogue systems [8] have demonstrated that dendrites always re-melt axially, from their tips downwards, as opposed to radially. This implies that the dominant diffusion path is from the dendrite tip to its root, as opposed to neighbouring dendrites of higher curvature. Consequently, secondary arms are eliminated from an array due to the variation in l of individual dendrites, not a variation in their radius of curvature, R_2. Kirkwood [6] has demonstrated that the rate of arm dissolution, $\mathrm{d}l/\mathrm{d}t$, can be related to the mean secondary arm spacing, $\bar{\lambda}_2$, in a straightforward manner. In this study we have used $\mathrm{d}l/\mathrm{d}t$ to measure the rate of dendritic ripening. This approach is valid as we are primarily concerned with the relative magnitudes of flow and diffusion effects.

For axial ripening via diffusional transport only, the ripening rate, $\mathrm{d}l/\mathrm{d}t$, is given by [30]

$$\frac{\mathrm{d}l}{\mathrm{d}t} = -\Xi D_\mathrm{l} \left(A_1 + A_2 \frac{D_\mathrm{s}}{D_\mathrm{l}} \right) \frac{1}{R_2^2} \qquad (13)$$

where R_2 is the radius of curvature at the tip of the secondary arm and A_1 and A_2 are geometrical factors relating to the diffusion paths through the liquid and solid respectively. Ξ is a group of material parameters which is given by

$$\Xi_t = \frac{\gamma_\mathrm{o} T_\mathrm{m} c_p}{H^2 \rho} \qquad (14)$$

for pure thermal coarsening or

$$\Xi_\mathrm{s} = \frac{\gamma_\mathrm{o} T_\mathrm{m}}{m H \rho C_\mathrm{l} (1-k)} \qquad (15)$$

for pure solutal coarsening. Here c_p is the specific heat capacity, m the slope of the liquidus, k the partition coefficient and C_l the solute concentration in the liquid. By considering the form of the modified transport Equation 12 and by dimensional analysis we may write

$$\frac{\mathrm{d}l}{\mathrm{d}t} = -\frac{\Xi D_\mathrm{l}}{R_2^2} \left\{ A_1 + A_2 \frac{D_\mathrm{s}}{D_\mathrm{l}} + A_3 P t_{fz} \right\} \qquad (16)$$

[1]CFX is a product of AEA Technology Ltd., Harwell, UK.

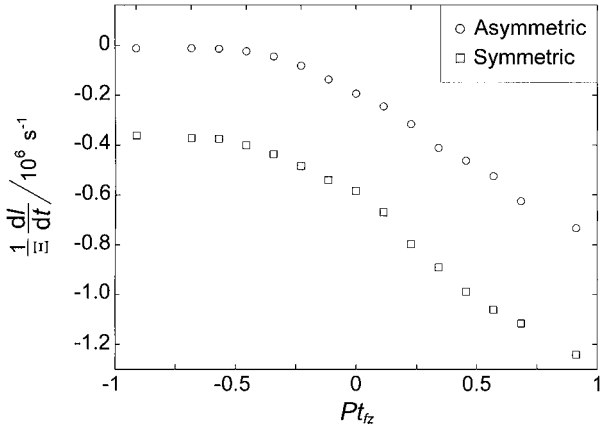

Figure 2 Ripening rate, dl/dt, as a function of the z-component of the flow velocity, V_{fz} for both the symmetric ($D_s = D_l$) and asymmetric ($D_s = 0$) ripening model.

where A_3 is a geometrical constant and Pt_{fz} is the Peclet number for the flow

$$Pt_{fz} = \frac{U_{fz} R_2}{D_l}. \tag{17}$$

Fig. 2 shows the ripening rate, dl/dt as a function of the Peclet number for the z-component of the flow velocity, V_{fz}. For both the symmetric ($D_s = D_l$) and asymmetric ($D_s = 0$) cases the curves show a linear increase in ripening rate with increasing Peclet number for positive flows (flow directed from the dendrite tip towards the root). Moreover, straight lines fitted through these portions of the data set are approximately parallel. For negative flows the linear trend continues provided the Peclet number is small. At large negative Peclet numbers the ripening rate attains a steady rate independent of the value of Pt_{fz}. The value of this steady rate is zero for the asymmetric case but non-zero in the symmetric case. That is, if fluid flow is in the same sense as diffusive transport the ripening rate will be enhanced whereas if the flow opposes the diffusive transport ripening will be inhibited. In the asymmetric case, at sufficiently high negative flow velocities, this diffusive transport can be completely inhibited and hence ripening cases. Conversely, in the symmetric case, ripening cannot be completely inhibited by the flow due to diffusion through the solid.

In the simulations presented all the dendrite arms within the array have the same initial value of R_2. In the figure presented this was $R_2 \approx 1\ \mu$m, although a sensitivity analysis has been conducted on R_2 to confirm the validity of Equation 16. Once the simulation begins R_2 may vary freely. However, because all the dendrites have the same initial curvature and the dominant dissolution mechanism is axial there is little competitive ripening and the value R_2 actually varies by only 12.5% during the course of the simulation. The initial secondary arm spacing in the simulations was taken as $\lambda_2 = 7.5\ R_2$, although due to the predominantly axial mass transfer direction the results are not particularly sensitive to the value of λ_2 assumed.

It is clear that Equation 16 provides a reasonable description of Fig. 2 provided we impose the additional constraint that

$$\frac{dl}{dt} = -\frac{\Xi D_l}{R_2^2}\left\{A_1 + A_2\frac{D_s}{D_l} + A_3 Pt_{fz}\right\} \quad \text{for} \quad A_1 \geq -A_3 Pt_{fz} \tag{18}$$

$$\frac{dl}{dt} = -\Xi\frac{A_2 D_s}{R_2^2} \quad \text{otherwise.} \tag{19}$$

That is, large negative flows cannot lead to negative ripening rates (i.e. growth) and for the symmetric model cannot cancel the effects of diffusion through the solid. The general validity of Equations 18 and 19 has be confirmed by a number of sensitivity studies.

Although our current model contains too few dendrites to be able to determine the coarsening exponent n in Equation 1 the form of the equations are consistent with $n = 1/3$ for pure diffusive ripening and $n = 1/2$ for pure advective ripening and these exponents can be obtained by a straightforward analytical analysis. This conclusion is insensitive to whether the axial coarsening model of Kirkwood [6] or the radial coarsening model [7] is used.

Kirkwood [6] has given $A_1 \equiv 4$, although a very simple geometrical model was assumed. Here we will endeavour to estimate the constants $A_1 - A_3$ from the results presented. From Fig. 2 the ripening rate at $Pt_{fz} = 0$ yields the coefficients A_1 from the curve for the asymmetric simulation and $A_1 + A_2$ from the curve for the symmetric simulation. These values are $A_1 = 0.46$ and $A_1 + A_2 = 1.39$ giving $A_2 = 0.93$. The value of A_2 can be confirmed independently by taking the base level of the symmetric ripening rate for $Pt_{fz} \ll 0$, which yields $A_2 = 0.88$. An independent evaluation of $A_1 + A_2$, obtained by varying D_l gave $A_1 + A_2 = 1.37$ indicating that the values obtained for A_1 and A_2 are self-consistent. The value of A_3 can be estimated from the slope of the linear portion of curves in Fig. 2 ($V_{fz} > 0$). These values are $A_3 = 1.44$ for the asymmetric simulation and $A_3 = 1.74$ for the symmetric simulation. Best estimates for these geometrical constants accordingly are $A_1 = 0.47 \pm 0.03$, $A_2 = 0.91 \pm 0.03$ and $A_3 = 1.59 \pm 0.15$. We would stress that these values are typical of 2-dimensional transport and will almost certainly be higher if a 3-dimensional transport model were considered.

These geometrical factors should scale in the same way as the dimensionless rate constants K_{diff} and K_{conv} discussed by Diepers *et al.* [26] for diffusional and convective coarsening respectively. It is interesting to note that in their calculation of 2-D Ostwald ripening the ratio K_{conv}/K_{diff} was 3.97 ± 0.33 (based on 6 simulations with solid fractions between 5.9% and 29.2%) which is not very different from our ratio $A_3/A_1 = 3.38$, despite the different geometries studied (Diepers *et al.* [26] used a solute based model so that diffusion was dominated by transport through the fluid phase in their model, consequently for comparison we have taken the geometrical factor for diffusion through the fluid phase, A_1, as being equivalent to their K_{diff}). This general agreement between our model and other models of coarsening with flow gives us reasonable confidence in

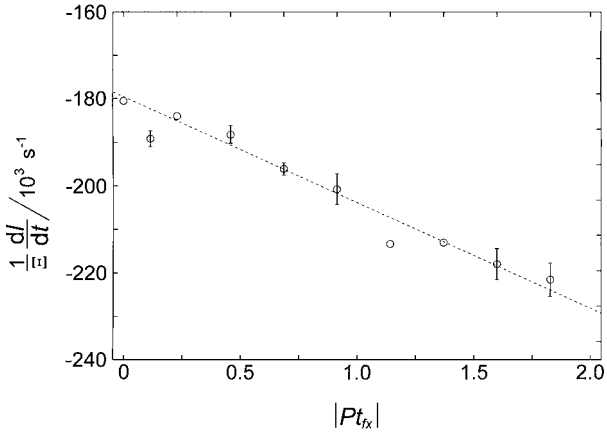

Figure 3 Ripening rate, dl/dt, as a function of the x-component of the flow velocity, V_{fx}. Error bars denote the difference between simulations with oppositely aligned flows.

our model, in particular with regard to the approximate nature of the flow-field used.

So far we have only considered the effects of flow directed along the axis of a secondary arm. According to the simple model proposed above a flow direct orthogonal to the axis of the secondary arm should have no effect. This hypothesis is investigated in Fig. 3, from which it is apparent that there is a small effect. For transverse flows (directed orthogonal to the axis of the secondary arm) any effect should be independent of the direction of the flow. Consequently we have plotted the ripening rate, dl/dt, against $|Pt_{fx}|$. For each data point the ripening rate has been calculated for both the positively and negatively directed flow and the mean value taken. The effect of transverse flow can be seen to be linear, suggesting that it has the same form as for flow directed along the axis. Consequently we may propose a modified form to Equation 18, namely

$$\frac{dl}{dt} = -\frac{\Xi D_l}{R_2^2}\left\{A_1 + A_2\frac{D_s}{D_l} + \boldsymbol{A}_3 \cdot \boldsymbol{Pt_f}\right\} \qquad (20)$$

where $\boldsymbol{Pt_f}$ is the (modified) vector Peclet number

$$\boldsymbol{Pt_f} = \frac{R_2}{D_l}\begin{pmatrix}|U_{fx}|\\ U_{fz}\end{pmatrix} \qquad (21)$$

and $\boldsymbol{A}_3$ is the vector

$$\boldsymbol{A}_3 = \begin{pmatrix}A_{3x}\\ A_{3z}\end{pmatrix} = \begin{pmatrix}0.05\\ 1.59\end{pmatrix} \qquad (22)$$

4. Discussion

So far we have considered how flow in the parent fluid may effect the dendrite arm coarsening process in a non-dimensional fashion. In this section we consider the magnitude of the flows that might actually arise in a dendritic semi-solid and consequently the nature of the flow related effects that might actually be observed. Hellawell [31] estimates that in metallurgical processing where the melt is subject to vigorous shearing, such as rheocasting, interdendritic flow velocities are likely to be of the order 0.01 m s^{-1}. Interdendritic flow velocities due to natural convection might be expected to be lower than this, possibly by up to an order of magnitude. From Fig. 2 we can estimate that values of Pt_{fz} around 0.5 will give rise to an effect comparable in magnitude to pure diffusional ripening. Taking order of magnitude estimates of $R_2 \approx 1\,\mu$m, $D_l \approx 10^{-9}$ m^2 s^{-1} for solutal diffusion or $D_l \approx 10^{-6}$ m^2 s^{-1} for thermal diffusion a Peclet number of 0.5 translates to a flow velocity, V_{fz}, of 10^{-3} m s^{-1} in a solutally controlled system or 1 m s^{-1} in a thermally controlled system. This would indicate that in solutally controlled systems (i.e., alloys under most solidification conditions) interdendritic flow by natural convection plays a significant role in the ripening of individual secondary arms. Conversely, it would also appear to rule out interdendritic flow having any significant effect on secondary arm coarsening in thermally controlled systems.

However, even though flow may have a significant effect on the ripening rate of individual secondary arms, this may not translate into a significant effect on the average secondary arm spacing, $\bar{\lambda}_2$. For macroscopic flows we would expect that in most cases the flow is randomly oriented with respect to the growth axis of the secondary arm. If the effect of flow on dl/dt were completely symmetric we would thus expect that, on average, macroscopic convection would have no effect on secondary arm spacing. Some arms would coarsen more quickly due to the flow but this would be exactly balanced by those coarsening less quickly. In fact, the effect is not exactly symmetric for two reasons. Firstly, if we consider the component of the flow aligned along the axis of the secondary arm (the z-direction in our numerical models), there is an upper limit to the extent to which dl/dt can be inhibited (the plateau in Fig. 2) but no corresponding limit to the extent to which it can be enhanced. High flow velocities will thus tend to shift the mean coarsening rate towards higher values. Secondly, transverse flows always lead to dl/dt being enhanced. However, the first of these mechanisms will only be operative for relatively high flow velocities while the second is a relatively minor contribution to the overall ripening rate. Randomly direct flows should thus lead to a small increase in $\bar{\lambda}_2$. Moreover, even where the flow direction can be controlled with respect to the direction of the primary dendrites, the four-fold symmetry of the secondary arms in cubic crystals should lead to an increased ripening rate. For a forced flow aligned along the primary trunk all the secondary arms will experience a transverse flow which will enhance ripening. Conversely, for a forced flow aligned transverse to the primary trunks, some of the secondary arms will have a component of the flow aligned along their growth axes and some component of the flow aligned transverse to their growth axes. Thus it is likely that under most flow condition the effect of flow on the mean secondary arm spacing, when scaled against the tip radius, will be to give rise to a small increase in $\bar{\lambda}_2$. This will be true even if there is a significant effect on the ripening rates of individual dendrites.

From the above arguments we would expect that the ripening rates under 1-g conditions should be slightly

higher than those under microgravity conditions. This conclusion is consistent with the data of Corrigan *et al*. [1]. From their results the ratio λ_2^c/λ_2^u can be calculated as 1.23 for the 1-*g* data set and 1.10 for the microgravity data set, where λ_2^c is the secondary arm spacing in the coarsening regime and λ_2^u is the secondary arm spacing in the uniform regime. That is, if we normalise against the secondary arm spacing in the uniform regime, where coarsening is negligible, dendrite grown under terrestrial conditions do show a slightly enhanced coarsening relative to those grown in microgravity.

Acknowledgements

The author is grateful to the Royal Society for their generous support under the University Research Fellowship Scheme.

References

1. D. P. CORRIGAN, M. B. KOSS, J. C. LA COMBE, K. D. DEJAGER, L. A. TENNENHOUSE and M. E. GLICKSMAN, *Phys. Rev*. E **60** (1999) 7217.
2. U. BISANG and J. H. BILGRAM, *ibid.* **54** (1996) 5309.
3. T. Z. KATTAMIS, J. C. COUGHIN and M. C. FLEMINGS, *Trans. Met. Soc. AIME* **239** (1967) 1504.
4. K. P. YOUNG and D. H. KIRKWOOD, *Met. Trans.* **6A** (1975) 197.
5. T. F. BOWER, HD. BRODY and M. C. FLEMINGS, *Trans. Metall. Soc. AIME* **236** (1966) 624.
6. D. H. KIRKWOOD, *Mater. Sci. Eng*. **73** (1985) L1.
7. U. FEURER and R. WUNDERLIN, "Fachbericht der Deutschen Gesellscaft für Metallknde" (Oberursel, FRG, 1977).
8. M. KAHLWEIT, *Scr. Metall*. **2** (1968) 251.
9. M. E. GLICKSMAN, N. B. SINGH and M. CHOPRA, *Mater. Res. Soc. Symp. Proc*. **9** (1982) 461.
10. M. H. JOHNSTON and C. S. GRINER, *Metall. Trans*. **8A** (1977) 77.
11. M. H. JOHNSTON and R. A. PARR, *Mater. Res. Soc. Symp. Proc*. **9** (1982) 651.
12. *Idem*., *Metall. Trans*. **13B** (1982) 85.
13. M. H. JOHNSTON, P. A. CURRERI, R. A. PARR and W. S. ALTER, *ibid*. **16A** (1985) 1683.
14. D. M. STEFANESCU, P. A. CURRERI and M. R. FISKE, *ibid*. **17A** (1986) 1121.
15. M. H. McCAY, J. E. LEE and P. A. CURRERI, *ibid*. **17A** (1986) 2301.
16. L. A. TENNERHOUSE, M. B. KOSS, J. C. LACOMBE and M. E. GLICKSMAN, *J. Cryst. Growth* **174** (1997) 82.
17. M. B. KOSS, J. C. LA COMBE, L. A. TENNENHOUSE, M. E. GLICKSMAN and E. A. WINSA, *Metall. Mater. Trans*. **30** (1999) 3177.
18. Q. LI and C. BECKERMANN, *Phys. Rev*. E **57** (1998) 3176.
19. *Idem*., *Acta Mater*. **47** (1999) 2345.
20. R. ANANTH and W. W. GILL, *J. Fluid Mech*. **208** (1989) 575.
21. R. TÖNHARDT and G. AMBERG, *J. Cryst. Growth* **194** (1998) 406.
22. D. M. ANDERSON, G. B. McFADDEN and A. A. WHEELER, *Physica* D **135** (2000) 175.
23. R. TÖNHARDT and G. AMBERG, *Phys. Rev*. E **62** (2000) 828.
24. X. TONG, C. BECKERMANN, A. KARMA and Q. LI, *ibid*. **63** (2001) 061601.
25. C. BECKERMANN, H.-J. DIEPERS, I. STIENBACH, A. KARMA and X. TONG, *J. Comp. Phys*. **154** (1999) 468.
26. H.-J. DIEPERS, C. BECKERMANN and I. STIENBACH, *Acta Mater*. **47** (1999) 3663.
27. A. R. MITCHELL and D. F. GRIFFITHS, "The Finite Difference Method in Partial Differential Equations" (Wiley, Chichester, 1980).
28. R. KOBAYASHI, *Physica* D **63** (1993) 410.
29. A. M. MULLIS, *Acta Mater*. **47** (1999) 1783.
30. *Idem*., *ibid*. **46** (1999) 4609.
31. A. HELLAWALL, in "4th International Conference on Semi-Solid Processing of Alloys and Composites," Sheffield 1996, edited by D. H. Kirkwood and P. Kapranos, p. 60.

Received 23 October 2001
and accepted 4 September 2002